Advances in Natural Sciences:
Nanoscience and Nanotechnology

Study on the nanocomposites of polyaniline and Zn doped Fe_3O_4 using for arsenic absorption in water

Adv. Nat. Sci.: Nanosci. Nanotechnol. **15** (2024) 035011 (8pp) https://doi.org/10.1088/2043-6262/ad6e5b

Study on the nanocomposites of polyaniline and Zn doped Fe_3O_4 using for arsenic absorption in water

Tran Minh Thi[1,2], Nguyen Mau Lam[3], Do Khanh Tung[4], Nguyen Manh Nghia[5], Duong Quoc Van[5], Vu Quoc Manh[6], Nguyen Thi Bich Viet[7], Duong Khanh Linh[7], Nguyen Thuy Chinh[8,9], Thai Hoang[8,9], Ştefan Ţălu[10] and Vu Quoc Trung[7]

[1] Institute for Theoretical and Applied Research, Duy Tan University, Hanoi 100000, Vietnam
[2] Faculty of Nature Science, Duy Tan University, Da Nang 550000, Vietnam
[3] Faculty of Physics, Hanoi Pedagogical University 2, Xuan Hoa Vinh Phuc 280000, Vietnam
[4] Institute of Materials Science, Vietnam Academy of Science and Technology, 18 Hoang Quoc Viet, Cau Giay, Hanoi 100000, Vietnam
[5] Faculty of Physics, Hanoi National University of Education, 136 Xuan Thuy, Cau Giay, Hanoi 100000, Vietnam
[6] Faculty of Pharmacy, Thanh Do University, Kim Chung, Hoai Duc, Hanoi 100000, Vietnam
[7] Faculty of Chemistry, Hanoi National University of Education, 136 Xuan Thuy, Cau Giay, Hanoi 100000, Vietnam
[8] Institute for Tropical Technology, Vietnam Academy of Science and Technology, Hoang Quoc Viet, Cau Giay, Hanoi 100000, Vietnam
[9] Graduate University of Science and Technology, Vietnam Academy of Science and Technology, 18 Hoang Quoc Viet, Cau Giay, Hanoi 100000, Vietnam
[10] The Directorate of Research, Development and Innovation Management (DMCDI), Technical University of Cluj-Napoca, 15 Constantin Daicoviciu St., Cluj-Napoca, 400020, Cluj country, Romania

E-mail: trungvq@hnue.edu.vn

Received 23 November 2023
Accepted for publication 24 July 2024
Published 27 August 2024

Abstract

The polyaniline/$Fe_{2.9}Zn_{0.1}O_4$ (PANI/$Fe_{2.9}Zn_{0.1}O_4$) nanoparticles with different mass ratios were synthesized by both co-precipitation and *in situ* polymerization methods. The FT-IR spectra and DTA analyses showed the involvement of PANI in the nanocomposite samples. The grain size of samples measured by SEM ranges from 25 to 40 nm. The magnetization of samples at 300 K, H = 11000 Oe decreased from 65 to 43 emu g^{-1} as PANI/$Fe_{2.9}Zn_{0.1}O_4$ mass ratio increased from 9% to 40%. At pH 7 and 300 K, the maximum arsenic (III) adsorption capacities of sample S_1 (mass ratio of 9%) $q_{max} = 43.48$ mg g^{-1} was higher than that of others and Fe_3O_4. Additionally, the substitution of Fe^{2+} ions by Zn^{2+} ions and the presence of PANI in samples contributed to improving the magnetic and chemical stability of samples over time. Furthermore, these materials could be reused after desorption in a solution at pH 14.

Keywords: adsorption ability, infrared spectra, magnetization, nanocomposites, polyaniline/$Fe_{2.9}Zn_{0.1}O_4$
Classification numbers: 2.01, 4.02, 5.02, 5.11, 5.18

1. Introduction

Nanocomposite materials comprising ferrite and polymer have garnered attention due to their wide range of applications in engineering [1, 2], biomedical applications [3–6], and water treatment [7–9] as well as environmental pollution monitoring [10–12]. In environmental treatment, magnetic nanocomposite materials are easy to recover and reuse, whereas the use of

nonmagnetic metal oxide hetero-structures, and mesoporous [13–17] poses significant challenges in recovery, often leaving residuals in the environment and causing secondary pollution. In this context, magnetic nanoporous materials are considered potential candidates for heavy metal ion removal due to their simple and efficient recovery using an external magnetic field. Iron oxide nanoparticles easily undergo a decrease in their physicochemical properties due to the rapid oxidation of Fe_3O_4 into γ-Fe_2O_3 as described by the equation:

$$4Fe_3O_4 + O_2 \rightarrow 6Fe_2O_3 \quad (1)$$

So, a large number of studies have focused on improving the magnetization and chemical stability of the nanomaterials by doping of M metal ions into $Fe_{3-x}M_xO_4$ (M = Mn, Co, Cu, Ni, Mg, Zn) [11, 18–25] for treating heavy metal ions, weak-acid oxyanion contaminants [9, 10, 26–28] or dyes in wastewater environments. Research results in [23] show that the magnetization (Ms) of Fe_3O_4 decreased from 69.5 emu g^{-1} to 56 emu g^{-1} after two synthesis months. Among the aforementioned Mx metal ions, the partial substitution of Zn for Fe ions in $Fe_{3-x}Zn_xO_4$ ($0 < x < 1$) has been shown to increase Ms compared to Fe_3O_4 [18, 29]. This corresponds to the reduction oxidation of the sample to γ-Fe_2O_3.

In addition, coating magnetic nanoparticles with polymers serves to preserve the chemical and physical characteristics of magnetic nanoparticles while facilitating their recovery and reuse as adsorbent materials [30, 31]. Polyaniline, known for its exceptional environmental stability, antioxidation, and anticorrosion properties, it can be easily blended with other oxides to form composite materials [32, 33].

In our previous publications, we investigated the maximum arsenic adsorption capacity (q_{max}) using Fe_3O_4, Mn^{2+}, Cu^{2+} doped Fe_3O_4 [23], and poly(1-naphthylamine)/Fe_3O_4 composites [31]. However, studies on the use of Mn^{2+}, Cu^{2+} doped Fe_3O_4 and the coating of magnetic nanoparticles with polyaniline (PANI), poly(1-naphthylamine) and polyvinyl pyrrolidone [29, 31, 34] have yielded disparate results, with little attention to the reusability of the materials. Additionally, the microscopic and magnetic properties of $Fe_{3-x}Zn_xO_4$ samples were studied, in which the samples had high magnetization [29]. In this research, we focus on studying the PANI/$Fe_{2.9}Zn_{0.1}O_4$ sample system with on the following aspects: (a) Microstructure analysis of nanocomposites with different PANI/$Fe_{2.9}Zn_{0.1}O_4$ mass ratios synthesized using a combination of the co-precipitation method and *in situ* polymerization method; (b) Investigating the effect of replacing Zn^{2+} ions for Fe^{2+} and PANI ions on the As adsorption capacity of PANI/$Fe_{2.9}Zn_{0.1}O_4$ nanocomposites as well as the desorption/re-adsorption capacities of the magnetic composite nanomaterials.

2. Experimental details

2.1. Chemical and apparatus

All chemicals were of analytical grade: $FeCl_3.6H_2O$, Na_2SO_3, 25% NH_4OH, $Zn(CH_3COO)_2{\cdot}2H_2O$, NaOH, HCl, acetone 99%, isopropanol (IPA), $(NH_4)_2S_2O_8$, As(III) solutions with an As(III) concentration of 106 ppb, ten times greater than the permissible values specified by the World Health Organization (WHO), were prepared from As_2O_3. The structure and morphology of the samples were investigated by x-ray Powder Diffraction (XRD) patterns (D5005, Bruker), Scanning Electron Microscopy (SEM) (S4800), Infrared Spectroscopy (IR Prestige −21), and Thermal Gravimetric Analysis (TGA) by DTG −60H. The magnetization of samples was measured using a vibrating sample magnetometer (VSM 8600 S). Additionally, BET analysis was conducted to determine the porosity and surface area of adsorbent materials, based on the inelastic interaction of adsorbent material and N2 gas at 77 K, using TriStar 3000 V6.07A and TriStar 3000 V6.08 software. The arsenic concentration of the solutions was determined using the Flame-Atomic Absorption Spectrophotometer (F-AAS 6300 Shimadzu) before and after the introduction of adsorbent magnetic nanoparticles.

2.2. Synthesis of $Fe_{2.9}Zn_{0.1}O_4$ by co-precipitation method

The initial chemicals, including HCl, $(CH_3COO)_2.Zn.2H_2O$, Na_2SO_3, $FeCl_3.6H_2O$, NH_3, $(NH_4)_2S_2O_8$ were high-purity chemicals sourced from Merck Chemical Company, Germany. Solutions of $FeCl_3{\cdot}6H_2O$, $Zn(CH_3COO)_2{\cdot}4H_2O$ containing Fe^{3+} and Zn^{2+} with a nominal Zn atom content of 0.10 were mixed and stirred together with the Na_2SO_3 solution. The synthesis steps for $Fe_{2.9}Zn_{0.1}O_4$ nanoparticles have been previously published in [29, 31].

2.3. Synthesis of PANI/$Fe_{0.90}Zn_{0.10}Fe_2O_4$ nanocomposites

The PANI/$Fe_{2.90}Zn_{0.10}O_4$ nanocomposite was synthesized via the *in situ* polymerization method, wherein the aniline monomers were adsorbed onto the surface of inorganic particles. Subsequently, aniline was polymerized by the catalyst $(NH_4)_2S_2O_8$ to form polyaniline (PANI). Following this, the inorganic particles were coated with PANI, precipitated, and separated from the solution. This synthesis method is briefly described as follows:

(a) A calculated amount of $Fe_{2.9}Zn_{0.1}O_4$ was added in 60 ml of distilled water, followed by 40 ml of IPA, and aniline. The mixture was then stirred for 60 min (mixture A).
(b) $(NH_4)_2S_2O_8$ solution was added dropwise to mixture A with a monomer/oxidizing agent molar ratio of 1:1.5 to obtain a black-blue mixture (mixture B). The mixture was allowed to stir for 2 h with an exothermal reaction
(c) Filter the mixture using an external magnet, then the obtained solid was dried by a Labconco Freeze concentrator for 5 h at 1 mPa and temperature of 40 °C. The samples with different mass ratios of PANI/$Fe_{2.9}Zn_{0.1}O_4$ were synthesized by *in situ* polymerization method of aniline on the surface of $Fe_{2.9}Zn_{0.1}O_4$ particles and coded by S_0, S_1, S_2, and S_3 as represented in table 1. The mass ratios of PANI/$Fe_{2.9}Zn_{0.1}O_4$ in the samples (in table 1) are re-calculated from the values of Ms measurements using VSM device.

Table 1. Aniline, PANI component in S_0, S_1, S_2, and S_3 samples.

Sample	S_0	S_1	S_2	S_3
$Fe_{2.90}Zn_{0.10}O_4$, (in g)	20	20	20	20
Aniline, (in ml)	0	1.8	5.1	7.8
Mass ratio (PANI/$Fe_{2.90}Zn_{0.10}O_4$), (in %)	0	9	26	40

2.4. The survey method of arsenic adsorption

The adsorption kinetic of the nanocomposites was studied by the nitrogen adsorption–desorption isotherms of S_0, S_1, S_2, and S_3 samples at 77K using BET method. The evaluation of the arsenic adsorption capacity of the samples was performed with different pH levels of As(III) solution at room temperature. Then, pH of the solution was selected at which As(III) adsorption occurs optimally to investigate q_{max} of the synthesized samples. The experiments were conducted by adding 0.01 g of samples (S_0, S_1, S_2, and S_3) into As(III) solutions of initial content of 106 ppb. Each mixture was then allowed to stir for 50 ÷ 60 min for complete adsorption. The arsenic contents before and after adsorption were analyzed by Flame-Atomic Absorption Spectrophotometer F-AAS.

3. Results and discussion

3.1. Structure and morphology

The XRD pattern of S_0 was presented in [29], wherein the substitution of Zn^{2+} with content of x = 0.10 caused a slight increase in the lattice constant (a = 8.39 A°) compared to Fe_3O_4 (a = 8.38 A°) [23, 29]. In figure 1, the diffraction peaks of (220), (311), (400), (442), (511), (440) of S_1, S_2 and S_3 were completely fitted with the standard diffraction pattern (JCPDS card No. 03–0863) of Fe_3O_4 [6] as well as in a previous publication [29], demonstrating a centered face cubic structure. This proves that the addition of polymer did not affect the crystal structure of the materials because PANI polymer is an amorphous material [34] and does not affect the crystal structure of $Fe_{2.9}Zn_{0.1}O_4$ nanoparticles. Using $2d\sin\theta = n\lambda$ [25], the lattice constants of the nanoparticles in the S_1, S_2, and S_3 samples were the same with a = 8.39 A° (in table 2).

The crystal sizes ($D_{x\text{-}ray}$) were calculated from XRD pattern about 11.8 nm of S_1, S_2, and S_3 samples using the formula $D = 0.9\lambda/\beta\cos\theta$ [25] (λ = 1.54 A°; and β is the full width at haft maximum of diffraction line).

In figure 2, the SEM image of S_1 shows the agglomeration in S_1 sample with grain size (D_{SEM}) from 20 to 30 nm due to the presence of PANI in the sample. Meanwhile, in SEM images of S_2, the borders of nanoparticles are more clearly with the grain sizes larger than S_1 sample (from 25 to 35 nm). However, the grain sizes of S_3 samples are about of 30 to 40 nm and larger than S_1 and S_2.

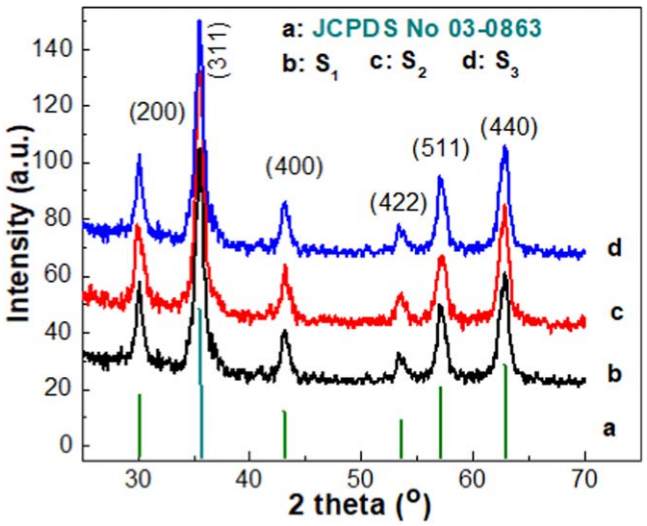

Figure 1. XRD patterns of S_1, S_2 and S_3.

Table 2. Vibrational modes observed in the FT-IR spectra of PANI, S_2 samples.

PANI in [35]		S_2
Wavenumber (cm^{-1})	Vibrational modes	Wavenumber (cm^{-1})
3124.5	vibrating of OH	3190.1; 3375.4
1573.5; 1492.6	vibrating of C = C group	1573.5; 1492.6
1400.3; 1303.9	vibrating of C-H, C-H^+	1400.3; 1303.9
1149.6	bending vibrating of C-H	1134.0
821.7; 594.1		571.0

3.2. FT-IR (Fourier-transform infrared spectroscopy) spectra analyses

The FT-IR spectrum of PANI (figure 3, line a) shows strongly absorbed peaks of PANI in the region from 1149.6 to 1573.5 cm^{-1} with the highest intensity at 1149.6 cm^{-1}. The peaks of 1149.6 cm^{-1}, 1303.9 cm^{-1}, 1400.3 cm^{-1}, 1492.6 cm^{-1}, 1573.5 cm^{-1} were attributed to the absorption of bending vibrating of C–H, and stretching vibrating of C–N^+ groups, C=C linkages in PANI [35], in table 2.

In work of [29] the FT-IR spectrum of PANI uncapped sample shows only the strong adsorbed peak at 571 cm^{-1}, along with two small peaks at 1400.3 cm^{-1}, 1623 cm^{-1}. Meanwhile, the vibrating peaks in the FT-IR spectrum of S_2 (figure 3, line b) appeared at 1573.5 cm^{-1}; 1492.6 cm^{-1}, 1303.9 cm^{-1} and 1134 cm^{-1}, with a slight shift of the peaks at 571 cm^{-1} and 1134 cm^{-1} peaks, suggesting the presence of PANI in the S_2 component. The vibrational modes observed in the FT-IR spectra of PANI, S_2 samples were shown in table 2.

3.3. TGA and DTG analyses

The TGA curve in figure 4(a) shows that at temperatures below 80 °C, PANI's mass drop was 13% owing to water

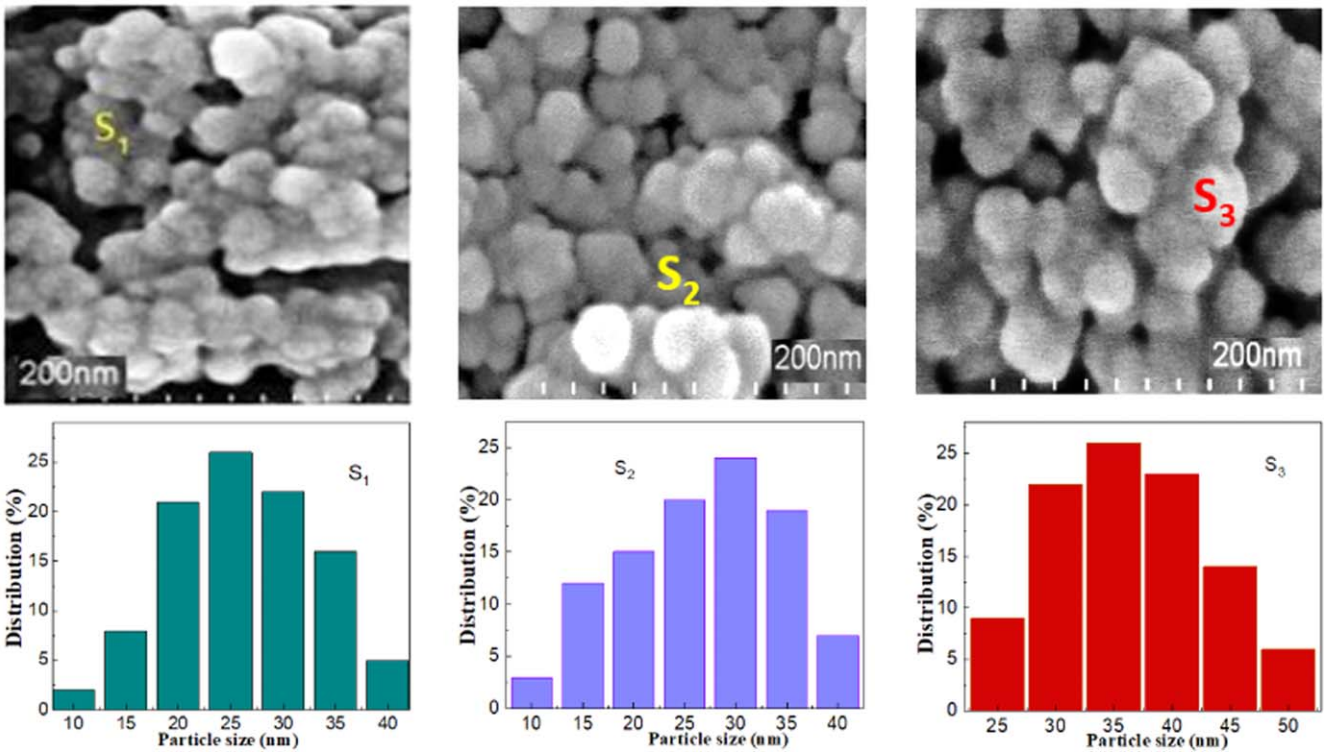

Figure 2. SEM images of S_1, S_2, S_3 and distribution of grain size.

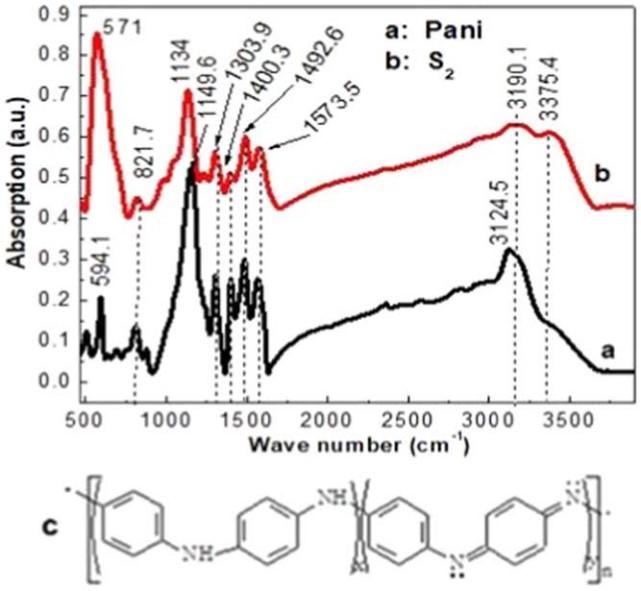

Figure 3. FT-IR spectra of samples (a) PANI, (b) S_2 and (c) PANI structure.

evaporation, with a prominent endothermic peak at 45 °C on the DTG curve. From 80 °C to 210 °C, the sample mass almost remained static. From 210 °C to 320 °C, the decrease in sample mass due to the decomposition of PANI to form monomers and oligomers, corresponding to a sharp endothermic peak at 292 °C in the DTG curve. At temperature over 320 °C, the weight loss it caused by the thermal decomposition of the oligomers. Complete decomposition of PANI occurs above 600 °C, as reported in [34].

The TGA curve of a typical S_2 sample in figure 4(b) also shows that at temperatures below 80 °C, there is an 8.6% reduction in sample mass due to water evaporation, corresponding to a sharp endothermic peak at 45.2 °C in the DTG curve. However, from 100 °C to 300 °C, the 3.3% drop in sample mass might be attributed to the breakdown of remaining monomers and oligomers. From 300 °C to 600 °C, the thermal decomposition of the oligomers causes a small and broad endothermic peak at 395 °C in the DTG curve. PANI is completely degraded at 600 °C, thus, the sample mass remaining at about 28%–29% at 600 °C is attributed to the remaining component of $Fe_{2.9}Zn_{0.1}O_4$. It can be observed that the DTG curve of S_2 compared to that of PANI suggest that PANI could interact with magnetic nanoparticles [34], leading to enhanced thermal stability of S_2 as well as the S_1 and S_3 samples up to 300 °C.

3.4. Magnetization and chemical instability

The Ms at H = 11000 Oe of S_0 is 74.5 emu g^{-1} [29], but Ms of S_1, S_2, and S_3 samples decreased from 65 emu g^{-1} to 43 emu g^{-1} due to the increase in PANI content (figure 5). Additionally, S_1, S_2, and S_3 samples have similar $Fe_{2.9}Zn_{0.1}O_4$ magnetic composition, so after synthesis, the PANI/$Fe_{2.9}Zn_{0.1}O_4$ mass ratios of in S_1, S_2, and S_3 samples are calculated as 9%, 26% and 40% as shown in table 1. These results are quite consistent with the mass loss observed in the typical S_2 sample by DTA measurement in figure 4. Furthermore, the specific mass of PANI is less than that of the ferromagnetic particles, thus, the larger particle sizes, the thicker the PANI shell and Ms of nanocomposites is even

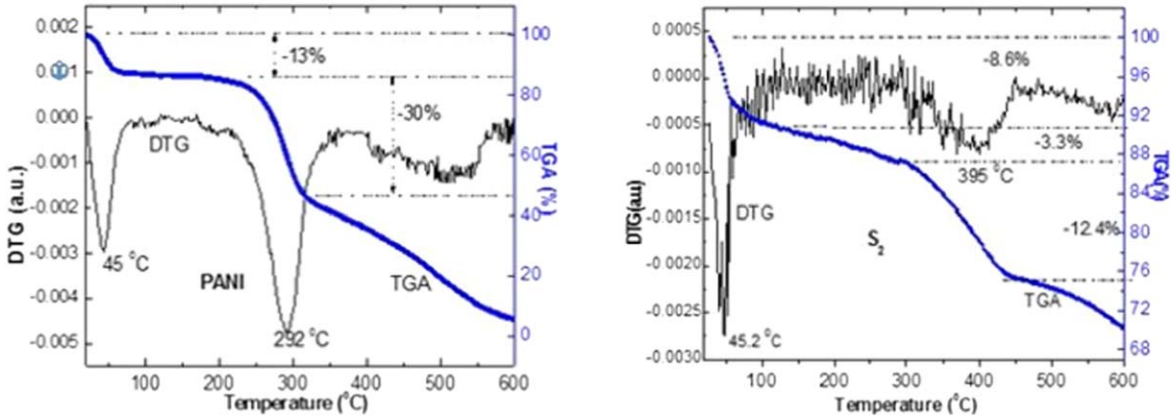

Figure 4. TGA and DTG analyses of samples: (a) PANI, and (b) S_2.

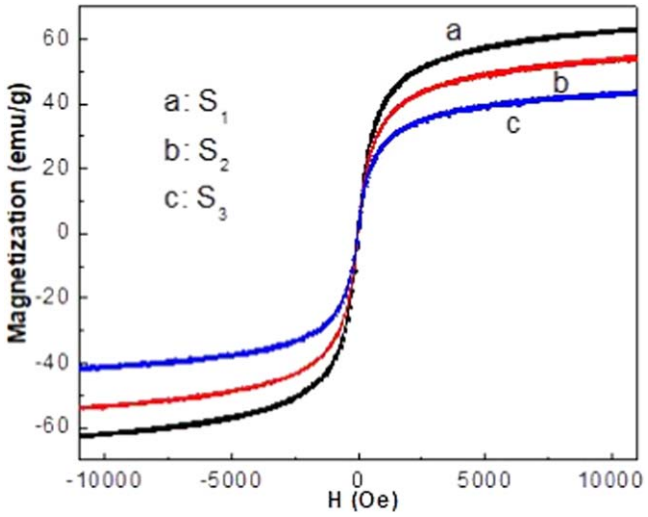

Figure 5. Magnetisation curves of S_1, S_2 and S_3.

smaller. However, due to the PANI coating, the magnetization and chemical properties of nanocomposite materials are more stable over time.

3.5. Porous properties, adsorption kinetic and arsenic adsorption capacity

Arsenic adsorption capacity is related to the pore properties and specific surface area of the samples. Therefore, the pore properties and specific surface areas of the samples were investigated. Subsequently, the arsenic adsorption capacity in different pH environments was examined. Based on these findings, the kinetics of adsorption are discussed using the observed results to determine the maximum As(III) adsorption capacity.

3.5.1. Porous properties of nanocomposite samples. The adsorption kinetics of S_0, S_1, S_2, S_3 can be explained on the basis of the inelastic exchange interaction between the specific surface area of the nanoparticle and the adsorbed material (N_2 gas molecule). Using this approach, the N_2 gas molecules connected to the nanoparticles before returning to the gas phase at 77 K [23, 31]. The delayed time is assumed to account for the phenomena of adsorption, as shown by the equation: $P/V_a(P_0 - P) = (1/V_m)(P/P_0)$ [36]. Whereas, V_a and V_m are, respectively, the amount of N_2 gas adsorbed at pressure P and when the surface area is fully covered in a mono-molecular layer, respectively. The N_2 adsorption–desorption isotherm curves of S_0, S_1, S_2, and S_3 samples with a mass of 0.54 g at 77 K were presented in figure 6. Using the BET (Brunauer, Emmett, and Taller) theory [36], BET desorption average pore diameter (D_{apd}) BET specific surface area (A_{sur}) of samples at a relatively low pressure $P/P_0 = 0.294$ were calculated as shown in table 3.

Comparing the specific surface area of the S_0 sample with that of the S_1, S_2, and S_3 composite samples, it can be observed that although the particle sizes of the S_1, S_2, and S_3 samples (approximately 25 nm to 40 nm as shown in the SEM images in figure 2) are larger than those reported for S_0 in previous work [29] (approximately 10 nm to 18 nm), PANI coating increased the porosity of the material. This resulted in achieving the highest specific surface area (94.7092 m^2 g^{-1}) for the S_1 sample with the appropriate PANI mass ratio.

3.5.2. The arsenic adsorption capacity in different pH environment. Initially, the S_0, S_1, S_2, and S_3 samples were investigated for As(III) adsorption in the environments with different pH at room temperature to determine the optimal pH level with the highest As(III) adsorption. By these observed results, the interaction characteristics in the As(III) adsorption process were analyzed to determine the kinetics of the As(III) adsorption process and determine the maximum As(III) adsorption capacity of the samples.

To investigate the pH effect on the adsorption capacity of the nanocomposite materials, the As(III) solutions with different pH ranging from 1 to 14 were prepared. The corresponding adsorption results were presented in figure 7.

After stirring the nanopowder-arsenic (III) solution mixture for approximately 50–60 min, it was observed from figure 7 that the remained arsenic (III) content varied with pH. Across all samples, the highest adsorption capacities were achieved within the pH range of 6–8.

In neutral media and pH below 9.2, the nanocomposites were stable with no iron (III), iron (II), and zinc (II) ions

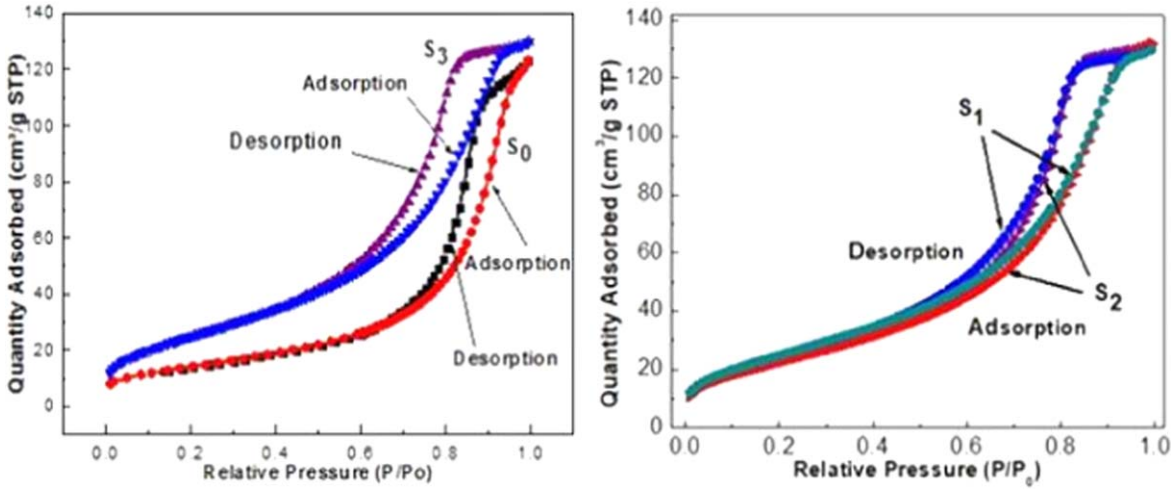

Figure 6. N_2 adsorption–desorption isotherm curves of samples.

Table 3. Porous properties and maximum arsenic adsorption ability.

Sample (this study)	BET D_{apd} (Å)	BET $A_{sur} \pm 0.02$ ($m^2\ g^{-1}$) ($P/P_o = 0.294$)	q_{max} (mg g^{-1})	Sample type in reference of other works	q_{max} (mg g^{-1}) in references
S_0	118.839	71.7685	41.49	Fe_3O_4 nanoparticles [7]	23.8 mg g^{-1}
				Nanoparticles with chemical agents [9]	11.76 mg g^{-1}
				Iron sludge [9]	12.74 mg g^{-1}
S_1	84.8842	94.7092	43.48	Fe_3O_4@SiO_2 nanoparticles [6]	16.58 mg g^{-1}
				Chitosan-magnetic-graphene oxide [37]	45 mg g^{-1}
S_2	88.1445	90.9667	40.06	Fe_3O_4 [23]	30.3 mg g^{-1}
				$Fe_{2.9}Mn_{0.1}O_4$ [23]	32.7 mg g^{-1}
				$Fe_{2.9}Cu_{0.1}O_4$ [23]	36.4 mg g^{-1}
S_3	94.6178	86.1750	34.48	Magnetic graphene nanoplatelet Fe@Fe_2O_3 nanoparticles [38]	11.34 mg g^{-1}

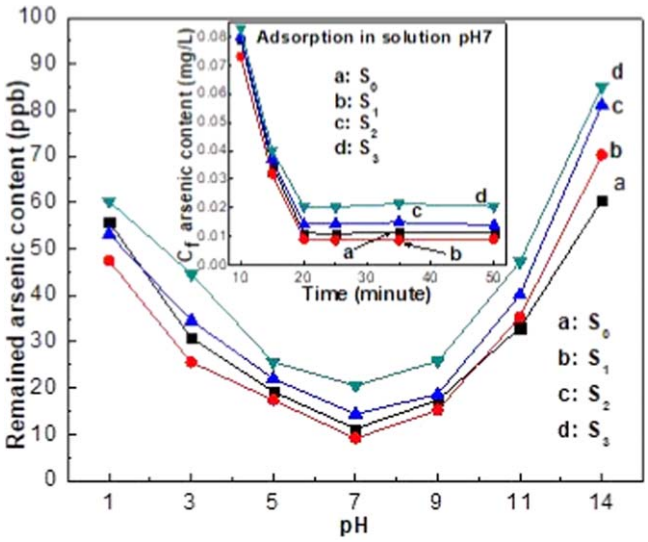

Figure 7. Remaining arsenic content as a function of pH. Inset: remained arsenic content C_f in solution at pH 7.

detected in the solution and the un-charge in the surface of As(III) (H_3AsO_3) [39], so at pH 7, the highest arsenic adsorption was occurred but not electrostatic interaction under this condition. Therefore, the As(III) adsorption was controlled by the surface complexation of composite nanoparticles at pH 7 media. Similar results were observed with other magnetic nanocomposites as reported earlier [37, 39].

In both strongly acidic and basic solutions, the adsorption capacity decreased. These issues are attempted to be explained by the characteristics of arsenic (III) at different pH media and the surface charge status of the nanocomposites in strong acidic or base environments [37]. At very low pH levels (pH from 1–2), the arsenic (III) adsorption is very less. That is attributed by the decomposition of the $Fe_{2.9}Zn_{0.1}O_4$ nanoparticles in strong acidic solution. However, at pH higher than the pH_{pzc} (~7), the surface of nanocomposites becomes negatively charged and As(III) exists mainly in form of $H_2AsO_3^-$, $HAsO_3^{2-}$, and AsO_3^{3-} anions [37, 39]. Consequently, the sharp decrease in the arsenic (III) adsorption capacity within the pH range of 11–14

can be attributed to the electrostatic repulsion between the negatively charged surface of the nanocomposites and the deprotonated anionic arsenic. However, this issue is subject to various discussions [37–41]. Nevertheless, the aforementioned experimental results suggest that the de-adsorption process of S_0, S_1, S_2, and S_3 should be conducted in a solution at pH 14 for reuse.

3.5.3. The kinetics of adsorption and maximum adsorption capacity in neutral environment. Based on the analyzed results above, the optimal adsorption of arsenic (III) occurs in a neutral environment (pH 7), where inelastic exchange interactions occur. These interactions stem from the Van der Waals forces between the magnetic nanoparticles and the adsorbent, as investigated by the Langmuir isotherm model at 300 K in a pH 7 environment [7, 8].

After each different stirring time interval, the equilibrium time of As(III) adsorption was analyzed in solution pH 7 (the inset of figure 7- after 10, 15, 20, 25, 35, and 50 min). The observed results show that the minimum time to reach adsorption equilibrium is 20 min in a pH 7 solution. Due to the porosity of the PANI coating nanocomposite samples, S_0 and inelastic collision in the adsorption process, the minimum adsorption equilibrium time is small compared with other iron sludge samples [9]. Unit of measurement of remaining arsenic (III) content C_f (in figure 7) is 1 ppb and in the inset of figure 7 is 1 mg L^{-1} (Note: 0.001 mg L^{-1} = 1 ppb and the permitted arsenic level is 10 ppb, according to regulations of the World Health Organization (WHO), the United States Environmental Protection Agency (USEPA) and the European Commission (EC). Langmuir isotherm equation at pH 7 and 300 K with the first-order linear relation was used to compute the q_{max} (mg g^{-1}) per unit mass of adsorbent at the equilibrium time [7, 8]:

$$C_f/q = \frac{1}{q_{max}}C_f + \frac{1}{b \times q_{max}} \quad (2)$$

where C_f is the remaining arsenic (III) content (mg l^{-1}) at equilibrium state; q (mg g^{-1}) is the adsorbed arsenic (III) amount per unit mass of adsorbent (S_0, S_1, S_2, and S_3) at the time of equilibrium; b (L.mg^{-1}) is constant attributed to the interaction of adsorbed arsenic (III) and adsorb compounds.

Figure 8 shows the dependence of C_f/q on C_f in the equilibrium state with a minimum adsorption time of 20 min at room temperature. As indicated in table 3, the maximum arsenic (III) adsorption capacities (q_{max}) of samples are 41.49 mg g^{-1}; 43.48 mg g^{-1}; 40.06 mg g^{-1} and 34.48 mg g^{-1}, respectively, with an error value of less than 5%. Thus, the q_{max} of S_1 sample was better than that of S_0 ($Fe_{2.9}Zn_{0.1}O_4$), sample as well as $Fe_{2.9}Mn_{0.1}O_4$, $Fe_{2.9}Cu_{0.1}O_4$ and Fe_3O_4 as reported in some works [7, 23, 31] under similar conditions. Additionally, the q_{max} value of S_1 is equivalent to the results in recent work (using chitosan magnetic graphene oxide nanocomposite) [37] and is larger than q_{max} values reported in other works (using core–shell Fe_3O_4@SiO_2 nanoparticles or magnetic graphene nanoplatelet with core–shell Fe@Fe_2O_3 nanoparticles) [6, 38]. The research results indicate that the combination of the co-precipitation method and *in situ* polymerization method is highly suitable for fabricating PANI/$Fe_{2.9}Zn_{0.1}O_4$ magnetic nanocomposite materials to meet wastewater treatment and other technical applications.

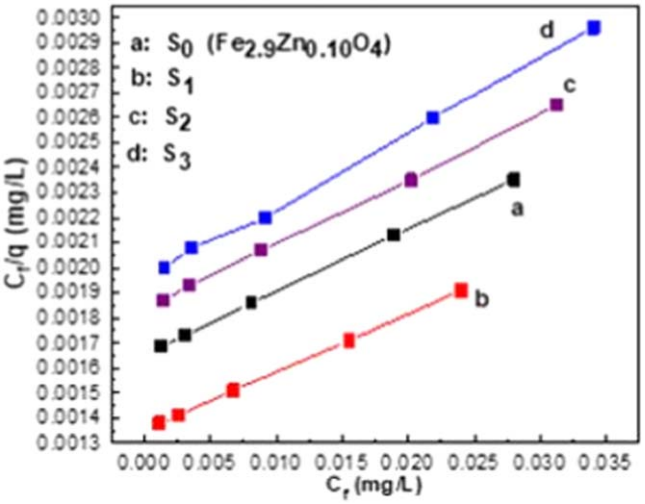

Figure 8. C_f /q dependence on C_f of S_0, S_1, S_2 and S_3.

4. Conclusion

The PANI/$Fe_{2.9}Zn_{0.1}O_4$ nanocomposite materials were successfully synthesized by a simple process with different mass ratios. These nanocomposite materials with large saturated magnetic moments and high specific surface area which contribute to their effective arsenic (III) adsorbing capability in aqueous. The optimal conditions for the adsorption process are at pH 7 and a minimum adsorption equilibrium time of 20 min. Among the samples, S_1 demonstrates the highest arsenic (III) adsorption capacity (q_{max} = 43.48 mg g^{-1}), surpassing that of S_0, S_2, and S_3 samples, as well as many other types of magnetic nanomaterials. Furthermore, the enhanced saturation magnetization by the partial substitution of Zn for Fe ions and chemical stability by PANI coating of the nanomaterials suggest their potential for adsorbing heavy metal ions at pH 7 and desorbing them in strong alkaline solutions with a pH 14, enabling the materials to be reused for further trials.

References

[1] Elamin N Y, Modwi A, Abd El-Fattah W and Rajeh A 2023 *Opt. Mater.* **135** 113323
[2] Patil V S, Thoravat S S, Kundale S S, Dongale T D, Patil P S and Jadhav S A 2023 *Chem. Phys. Lett.* **814** 140334
[3] Singh C, Sharma S, Jaglan S, Aphesteguy J C, Jacobo S, Abdel-Latif I A, Albargi H B, Kaur R, Singh J and Sharma. S 2023 *IEEE Trans. Nanobiosci.* **22** 582–9
[4] Fizesan I *et al* 2021 *Pharmaceutics* **13** 2148
[5] Mohamed A A K *et al* 2020 *Int. J. Mol. Sci.* **21** 7775
[6] Xu J, Sun Y and Zhang J 2020 *Sci. Rep.* **10** 16026
[7] Khodabakhshi A, Amin M M and Mozaffari M 2011 *Iran J. Environ. Health. Sci. Eng.* **8** 189

[8] Ruijiang L, Yi L, Xiangqian S, Xinchun Y, Xuewen C and Yingying G 2013 *J. Nanosci. Nanotechnol.* **13** 2835
[9] Huiping Z, Longxue Z, Tongda Q, YapingY, Jie Z and Dong L 2020 *Sci. Rep.* **10** 9335
[10] Asgharinezhad A A, Esmaeilpour M and Siavoshani. A Y 2022 *RSC Adv.* 2022 **12** 19108–14
[11] Shah M T, Alveroglu E and Balouch A 2018 *J. Alloys Compd.* **767** 151
[12] Lixin Y *et al* 2018 *J. Alloys Compd.* **748** 111
[13] Ţălu Ş 2015 *Micro and Nanoscale Characterization of Three Dimensional Surfaces. Basics and Applications* (Napoca Star Publishing House)
[14] Xiaolong L, Fengqin Z, Chao M, Elingarami S and Nongyue H 2012 *J. Nanosci. Nanotechnol.* **12** 2939
[15] Zapotoczny B *et al* 2012 *J. Nanomater.* **2012** 341073 1-7
[16] Méndez-Rodríguez L, Zenteno-Savín T, Acosta-Vargas B, Wurl J and Imaz-Lamadrid M 2013 *Nat. Sci.* **5** 238
[17] Kuen-Song L, Khalilalrahman D, Yeu-Jye L, Hua K and Pei-Ju H 2013 *J. Nanosci. Nanotechnol.* **13** 2675
[18] Park J W, Jang A N, Song J H, Park C Y and Lee Y S 2013 *J. Nanosci. Nanotechnol.* **13** 1895
[19] Zaki H M *et al* 2013 *J. Nanosci. Nanotechnol.* **13** 4056
[20] Larumbe S *et al* 2012 *J. Nanosci. Nanotechnol.* **12** 2652
[21] Deepshikha R, Rajnish K and Pandey R K 2013 *J. Nanosci. Nanotechnol.* **13** 812
[22] Putri W B K *et al* 2023 *Adv. Nat. Sci.: Nanosci. Nanotechnol.* **14** 015003
[23] Thi T M, Trang N T H and Anh N T V 2015 *Appl. Surf. Sci.* **340** 166
[24] Aparna M L, Grace A N, Sathyanarayanan P and Sahu N K 2018 *J. Alloys Compd.* **745** 385
[25] Sudheesh V D *et al* 2018 *J. Alloys Compd.* **742** 577
[26] Uwamariya V, Petrusevski B, Slokar Y M, Aubry C, Lens P N L and Amy G L 2015 *Water Air Soil Pollut.* **226** 184
[27] Hristovski K D and Jasmina M 2017 *Sci. Total Environ.* **598** 258
[28] Huda F, Yi-Fong P and Tsair-Fuh L 2015 *Water Air Soil Pollut.* **226** 14
[29] Thi T M, Trung V Q, Tung D K, Thanh P T, Yen N H and Lam N M 2021 *Jpn. J. Appl. Phys.* **60** 025001
[30] Sadia A, Shaheer A M, Young S K, O-Bong Y and Hyung-Shik S 2010 *Colloid Polym. Sci.* **288** 633
[31] Minh Thi T, Thi Huyen Trang N, Quoc Trung V and Minh Vuong N 2016 *Front. Mater. Sci.* **10** 56
[32] Li Z and Gong L 2020 *Materials* **13** 548
[33] Beygisangchin M, Abdul Rashid S, Shafie S, Sadrolhosseini A R and Lim H N 2021 *Polymers* **13** 2003
[34] Gabal M A, Al-Juaid A A, El-Rashed S, Hussein M A and Al Angari Y M 2018 *J. Alloys Compd.* **747** 83–90
[35] Bogdan B, Andreea G, Paul D, Adriana B and Valentin B 2017 *Polymers* **9** 732
[36] Paul A W and Clyde O 1997 contributors Ronnie W C, James P O and Simon Y Y *Analytical Methods in Fine Particle Technology* (Micromeritics Instrument Corporation) 60
[37] Sherlala A I A, Raman A A A, Bello M M and Buthiyappan A 2019 *J. Environ. Manage.* **246** 547
[38] Jiahua *et al* 2012 *ECS J. Solid State Sci. Technol.* **1** M1–5
[39] Su H, Ye Z and Hmidi N 2017 *Colloids Surf. A Physicochem. Eng. Asp.* **522** 161
[40] Blain P, Vyom P and Ajay M 2015 *Environ. Sci. Water Res. Technol.* **1** 77
[41] Yu F, Sun S, Ma J and Han S 2015 *Phys. Chem. Chem. Phys.* **17** 4388